

Properties of satellite galaxies in the SDSS photometric survey: luminosities, colours and projected number density profiles.

M Lares, D G Lambas and M J Dominguez

Instituto de Astronomía Teórica y Experimental (CONICET-UNC). Observatorio Astronómico de Córdoba (UNC), Laprida 854, X5000BGR, Córdoba, Argentina

mlares@mail.oac.uncor.edu

ABSTRACT

We analyze photometric data in SDSS-DR7 to infer statistical properties of faint satellites associated to isolated bright galaxies ($M_r < -20.5$) in the redshift range $0.03 < z < 0.1$. The mean projected radial number density profile shows an excess of companions in the photometric sample around the primaries, with approximately a power law shape that extends up to $\lesssim 800kpc$. Given this overdensity signal, a suitable background subtraction method is used to study the statistical properties of the population of satellites, down to magnitude $M_r = -14.5$. We have also considered a colour cut consistent with the observed colours of spectroscopic satellites in nearby galaxies so that distant redshifted galaxies do not dominate the statistics. We have tested the implementation of this background subtraction procedure using a mock catalogue derived from the Millenium simulation based on a Λ CDM model. We find that the method is effective in reproducing the true projected radial satellite number density profile and luminosity distributions, providing confidence in the results derived from SDSS data. We find that the spatial extent of satellite systems is larger for bright, red primaries. Also, we find a larger spatial distribution of blue satellites. For the different samples analyzed, we derive the average number of satellites and their luminosity distributions down to $M_r = -14.5$. The mean number of satellites depends very strongly on host luminosity. Bright primaries ($M_r < -21.5$) host on average ~ 7 satellites with $M_r < -14.5$. This number is reduced for primaries with lower luminosities ($-21.5 < M_r < -20.5$) which have less than 2 satellites per host. We provide Schechter function fits to the luminosity distributions of satellite galaxies where the resulting faint end slopes lie in the range 1. to 1.3, consistent with the universal value. This shows that satellites of bright primaries lack an excess population of faint objects, in agreement with the results in the Milky Way and nearby galaxies.

1. Introduction

According to the currently accepted model of structure formation, galaxy systems arise as the result of hierarchical clustering (White & Frenk 1991; Bertschinger 1994; Cole et al. 1994). The details by which galaxies form and evolve in dense or moderately dense environments, where galaxy-galaxy interactions are frequent and matter distributes in a rich substructure, depend on the characteristics of those environments. The assembly of galaxy systems entail the process of matter accretion, governed by gravity, as well as astrophysical phenomena, such as the efficiency of gas to cool and collapse or the energy feedback related to the late stages of stellar evolution (Viola et al. 2008; Kang et al. 2006). Some of these details are not yet fully understood, and observational evidence is fundamental to constraint structure formation and evolution models, specially because faint galaxies are more sensitive to astrophysical processes like supernova feedback and ram pressure stripping. In particular, statistical studies of systems of galaxies are key to understand the transformations of galaxies due to the interactions between galaxies and their environment (Nichol et al. 2003).

Although the formation of a galaxy is believed to take place on the potential well of a dark matter halo, not all haloes host a galaxy. As pointed out first by Klypin et al. (1999), the number of halos in numerical simulations were an order of magnitude greater than the observed number of satellites in the local group (Moore et al. 1999; Kravtsov et al. 2004; Strigari et al. 2007). This difference has been a matter of lively debate, being attributed either to a lack of observed galaxies or to an excess of formed objects in simulations. Willman et al. (2002) discussed the possibility of under counting satellite galaxies in the Milky Way and estimated the actual number of satellites in about twice the known population at that time. The authors argued that galactic extinction and stellar foreground can lead up to 33% of incompleteness, and then the number of Milky Way satellites at low galactic latitude and at galacto-centric distance might be underestimated. Simon & Geha (2007) found that the number of satellites in the Milky Way system was greater than previously expected, based on an analysis of the SDSS data. With these findings, the discrepancy between the number of observed and simulated satellites reduces to a factor of nearly 4.

The distribution of satellite luminosities is also key to the development of models and understanding of the processes of galaxy formation (Benson et al. 2003; Benson et al. 2004; Okamoto et al. 2010). Given the low luminosity of most satellites, however, their observation is usually onerous and hardly accessible outward of the Local Group. Mateo (1998) put forward a detailed census of dwarf galaxies, from which a flat faint end of the luminosity function in the Local Group could not be discarded. Background subtraction methods have been widely used to obtain galaxy luminosity function in clusters. While some authors report results of this procedure on individual clusters (Oemler 1974). Since it is not limited to

the computation of luminosities, it can be also used to obtain the color-magnitude relation (Pimbblet 2008). Andreon et al. (2005) present a variation of the background decontamination method, avoiding the use of arbitrary binning and incorporating the background noise as part of a refined model for the description of data. Koposov et al. (2008) presented a search methodology for Milky Way satellite galaxies in SDSS data through the computation of efficiency maps. Search for stellar concentrations using these maps suggest a luminosity distribution that steadily rises following a power law up to $M_v \simeq 5$. From there on, a flat distribution could not be discarded (Koposov et al. 2008).

Tollerud et al. (2008) use completeness limits for the SDSS-DR5 to implement a correction for luminosity bias. Although a first order correction would produce an increase in the faint end of the luminosity function, the authors bring forward that this result is not well enough constrained given available data. Trentham & Tully (2002) study the faint end of the galaxy luminosity function in five different local environments, from the Virgo cluster to NGC 1023 group. The authors derive an averaged luminosity distribution in the range $-18. < M_r < -10$ (Cousins R magnitude) and infer a faint end slope $\alpha \sim -1.2$. In the particular case of NGC 1023, a more detailed study confirmed later that the faint end is consistent with a shallow slope (Trentham & Tully 2009). Tully & Trentham (2008) studied the NGC 5353 group and attributed a faint end slope $\alpha = -1.15$ to the fact that this group is at an intermediate evolutionary age.

Membership of individual galaxies through spectroscopic measurements is inefficient in terms of observing time, given the large fraction of background objects that have to be rejected. This results in few systems with derived luminosity function complete down to faint magnitudes. For this reason, a background subtraction technique is an efficient method to study, on a statistical basis, properties of the population of companion objects. Using deep mock catalogues constructed from a numerical simulation, Valotto et al. (2001) analyze systematic effects in the determination of the galaxy luminosity function in clusters. Their results indicate a strong tendency to derive a rising faint end when clusters are selected without redshift information. This is due to projection effects, since many of the clusters selected in 2D have no significant counterpart in 3D. Muñoz et al. (2009) use Mock catalogues constructed using GALFORM (Baugh 2006) semianalytic model of galaxy formation to study the reliability of the statistical background subtraction method to recover the underlying observer-frame luminosity function of high redshift ($z \simeq 1$) cluster galaxies in the K_s band. These authors find that the optimal response of the method in recovering the underlying galaxy luminosity function occurs when background corrected counts of faint galaxies are complemented with photometric redshifts of bright galaxies. They also show that the increase in the number of galaxy clusters that contribute to the computations dramatically reduce stochastic errors. Christlein (2000) study luminosity functions for galaxies

in loose groups and suggests that the ratio of dwarf to giant galaxies is continuously increasing from low to high mass groups. This is based on data from the Las Campanas Redshift Survey, where environment is estimated using the line-of-sight velocity dispersion of the host groups. Background subtraction has been applied to single clusters (Andreon et al. 2005; Barkhouse et al. 2007) and to ensembles of clusters (González et al. 2006).

The goal of this work is to obtain statistical properties of satellite galaxies in the magnitude range $-18.5 < M_r < -14.5$, using SDSS photometric data. Previous studies of galaxy satellites concern mostly Milky Way and nearby galaxies, so that this work complements with a study of projected radial number density profiles, luminosity, and colour distributions for a statistically large sample of primaries within $z = 0.1$. The definitions of host samples and the adopted satellite selection criteria are presented in section 2. The details of the background subtraction procedure are given in section 3. Then, in section 4 we present the derived distributions of satellite properties. In order to validate the implemented method, we test it in section 5. Finally, the main conclusions are provided in section 6.

2. Photometric and spectroscopic data

We use the large database provided by the Sloan collaboration (SDSS, Stoughton et al. 2002), which provides photometric information of objects down to faint magnitudes. This survey has been carried out using a dedicated 2.5m telescope (Gunn et al. 2006), and comprises digital photometric information of stars and galaxies in 5 bands (Fukugita et al. 1996; Smith et al. 2002) reduced by an automated pipelines (Lupton et al. 2001). The limiting magnitude is 22.2 in the r -band. A set of the brightest and more concentrated galaxies in the main galaxy sample has been selected for spectroscopic follow up (Blanton et al. 2003). This leads to the spectroscopic galaxy catalogue, which contains galaxies with Petrosian magnitude $r < 17.77$ (Strauss et al. 2002). Both photometric and spectroscopic data are accessible through a web interface to the public releases of the survey. The latest release comprises nearly 18 Tb of catalogued data for objects identified as galaxies by the automated data reduction pipeline (Data Release 7, Abazajian et al. 2009). The main galaxy sample in DR7 comprises 691055 galaxies with 95% completeness down to a limiting magnitude $r_{lim} = 17.77$ in the r -band. The surface brightness limits are imposed by the instrument capabilities and the automated reduction pipeline, so that these data sets allow to retrieve information about galaxies above the surface brightness limit of the catalogue, $\mu_{50} \leq 24.5 \text{ mag arcsec}^{-2}$ in the Petrosian r -band (Strauss et al. 2002). All galaxies in this sample have redshift measurements and serve as primary targets for the study of fainter galaxies, accessed from a deeper photometric sample. In this work we obtain statistical properties of faint satellites, most of

them not present in the spectroscopic survey, associated to primaries with measured redshifts in the range 0.03 to 0.1. To this aim, we use the New York Value Added Galaxy Catalog (NYU-VAGC, Blanton et al. 2005) to extract photometric information of neighboring galaxies of primaries. This catalogue is based on the sixth release of the Sloan Digital Sky Survey, and covers 9583 deg^2 of sky distributed into a northern cap and three southern stripes. We notice that the sky coverage of the main galaxy sample in DR7 is approximately included in the NYU-VAGC DR6 area, so that the cross-correlation between these two catalogues is suitable for the purpose of this work.

2.1. Host samples and galaxy selection criteria

We have considered primaries brighter than $M_p = -20.5$ (r -band luminosities) in the redshift range 0.03 to 0.1, applying an isolation criterion in order to avoid high density environments such as pairs or groups of galaxies. The density contrast around galaxies fainter than $M_p = -20.5$ is low and comparable to Poisson uncertainty. Since the method, detailed in section 3, is based on the presence of a strong signal to background, we left them out of consideration in defining the samples of hosts. These primaries are constrained to have no neighbors brighter than $M_p + 2$ within projected distance 700 kpc and relative radial velocity difference 700 km/s. These criteria are similar to those adopted in previous studies using spectroscopic samples (Sales & Lambas 2005; Chen et al. 2006; Agustsson & Brainerd 2010), and are intended to select and isolate halos where a dominating, assumed central galaxy of the satellite system is found. The total sample of primaries comprises 51710 objects brighter than $M_p = -20.5$ in the redshift range 0.03 to 0.1.

Taking into account galaxy luminosities and colours, we have considered different subsamples of primaries in order to explore possible dependencies of the satellite properties as a function of host properties. The description of the subsamples considered is given in table 1. Subsample names are indexed on a three character basis: a number indicating the host luminosity selection ("0" for full sample, "1" for hosts with $-22.0 < M_r < -21.0$, and "2" for hosts with $M_r < -21.5$); and two letters indicating host and satellite colours. For simplicity, uppercase characters correspond to primary galaxy colours (A,R,B: All, Red, Blue), while lowercase indicate satellite colours (a, r, b standing for all, red and blue respectively). In figure 1 we show the distributions of r -band absolute magnitudes, $g - r$ colours and redshifts of hosts in the total sample. The bimodal distribution of primary galaxy colours can be clearly appreciated, and we use a colour cut $g - r = 0.8$ to separate subsamples according to host colour.

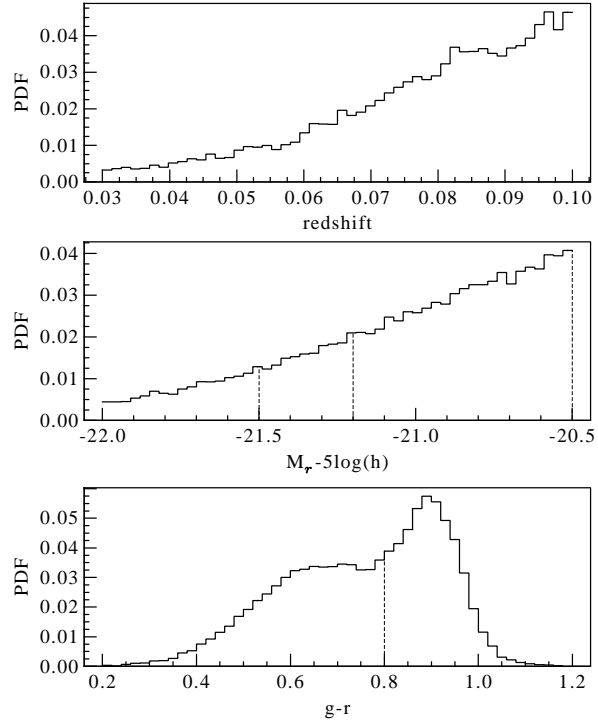


Fig. 1.— Properties of primary galaxies in the total sample. This sample comprises 51710 galaxies brighter than $M_r = -20.5$ in the redshift range 0.03 to 0.1, satisfying the isolation criteria stated in section 2.1.

sample	primaries			galaxies	
	luminosity	colour	N_p	R_{max} [kpc]	colour
S0-A-a	$M_r < -20.5$	all	51710	< 800	$-0.4 < g - r < 1.0$
S0-A-r	$M_r < -20.5$	$g - r > 0.8$	51710	< 800	$0.4 < g - r < 1.0$
S0-A-b	$M_r < -20.5$	$g - r < 0.8$	51710	< 800	$-0.4 < g - r < 0.4$
S1-A-a	$-21.5 < M_r < -20.5$	all	42335	< 300	$-0.4 < g - r < 1.0$
S1-A-r	$-21.5 < M_r < -20.5$	$g - r > 0.8$	42335	< 300	$0.4 < g - r < 1.0$
S1-A-b	$-21.5 < M_r < -20.5$	$g - r < 0.8$	42335	< 1000	$-0.4 < g - r < 0.4$
S2-A-a	$M_r < -21.5$	all	9375	< 1200	$-0.4 < g - r < 1.0$
S2-A-r	$M_r < -21.5$	all	9375	< 1000	$0.4 < g - r < 1.0$
S2-A-b	$M_r < -21.5$	all	9375	< 1500	$-0.4 < g - r < 0.4$
S2-R-a	$M_r < -21.5$	$g - r > 0.8$	4740	< 1500	$-0.4 < g - r < 1.0$
S2-R-r	$M_r < -21.5$	$g - r > 0.8$	4740	< 1000	$0.4 < g - r < 1.0$
S2-R-b	$M_r < -21.5$	$g - r > 0.8$	4740	< 1500	$-0.4 < g - r < 0.4$
S2-B-a	$M_r < -21.5$	$g - r < 0.8$	4635	< 700	$-0.4 < g - r < 1.0$
S2-B-r	$M_r < -21.5$	$g - r < 0.8$	4635	< 700	$0.4 < g - r < 1.0$
S2-B-b	$M_r < -21.5$	$g - r < 0.8$	4635	< 1000	$-0.4 < g - r < 0.4$

Table 1: Definition of satellite samples considering colour range, maximum projected distance to the primary and primary properties. The number of primaries N_p of each sample is also indicated. Satellite galaxies have a lower bound of $g - r = -0.4$ for samples *a* and *b*. Upper case letters A, B and R stand for All, Blue and Red, respectively. Similarly, lower case letters indicate the ranges of satellite colours.

3. Background subtraction method

Background subtraction methods are based on the simple idea of counting the number of objects in a region where a given signal is expected to lie, superposed to an uncorrelated noise, and subtracting a statistical estimation of that noise. In this case, the signal is due to the presence of satellite galaxies in systems dominated by a central and luminous galaxy, and the noise is associated to the background and foreground galaxies not dynamically linked to that primary galaxy. Then, it allows to statistically obtain properties of the faint galaxies associated to the primaries, without the need of redshift information for individual objects. This is accomplished provided that the working hypothesis of the central primary is satisfied and convenient ranges of observed parameters are chosen so that to minimize the contribution of background counts. Although the method does not allow to quantify the contribution to the signal of each individual object, it is possible to obtain statistical estimates of probability density distributions describing galaxy properties. This is accomplished by restricting galaxies to a fixed bin of the variable, for instance the luminosity of the satellite or their distance to the central galaxy, and normalizing to the number of contributing systems in that bin, after implementing the background subtraction.

Within the hierarchical clustering paradigm, the matter distribution can be roughly described by a set of halos populated with galaxies, according to certain recipes that depend on galaxy type (Cooray & Sheth 2002). This model can give insight to adopt an appropriate choice of the centers, which is key to increase the signal from the satellite population against the background noise and obtain reliable results using this method. Central galaxies play a different role than the rest of objects within the halo due to its particular accretion history, related to the merging of massive galaxies in each halo, and eventually the accretion of most of the available gas and even other minor galaxies (Cooray & Milosavljevic 2005). While galactic cannibalism has been proposed as the main mechanism for building up central galaxies (Ostriker & Tremaine 1975; White 1976; Vale & Ostriker 2006), it has also been suggested that major mergers (Lin et al. 2004) and dry mergers (Liu et al. 2009; Khochfar & Silk 2009) play an important role in the different stages of their evolution. From a dynamic point of view, relative velocities of central galaxies with respect to the halos in which they reside are very small, compared to the large velocity dispersion of satellite galaxies. This leads to a clear observational distinction between central and satellite galaxies (Vale & Ostriker 2006). It is also known that a central galaxy is often the most luminous galaxy within their halo (Vale & Ostriker 2006). Even when this "central galaxy paradigm" has been claimed to be inaccurate (Skibba et al. 2010), specially in high mass systems, the precise location of the center of the halo is not crucial for the implementation of the method, since it integrates galaxy counts in a region where overdensity signal is clearly present. Still, the location of the brightest galaxy in this special type of galaxy systems, where a galaxy strongly dominates

in luminosity and the total mass of the systems is quite low, is a very good approximation to the position of the center of the galaxy system. Under these assumptions, the brightest galaxies are expected to reside in the centers of haloes (Jones & Forman 1984; Lin et al. 2004; Smith et al. 2005), and can be used statistically to analyze galaxy overdensities associated to satellites. Accordingly, we limit the sample of centers to bright isolated galaxies, since they are likely central galaxies of small haloes.

The main requirement for the success of this procedure is a significant mean overdensity around a given sample of primaries. This fact leaded us to consider bright galaxies ($M_p < -20.5$) since fainter primaries do not show a significant density enhancement suitable for statistical background subtraction. The uncertainty in the background decontamination procedure is dominated by Poissonian statistics of large number subtractions. A significant increase in the signal to noise ratio can be achieved by eliminating those galaxies with a low probability of association to the primaries. Colour distributions for SDSS satellite galaxies derived from the spectroscopic sample in three different absolute magnitude bins between -18.5 and -14.3 are given in figure 2, from which it can be appreciated that a colour cut in $g - r < 1$ is likely to include most of faint companion objects and has the advantage of removing high redshift galaxies reddened by K-correction. Therefore, in all computations we exclude objects redder than this threshold to lower the noise due to the presence of high redshift galaxies. A clear indication that our colour cut $g - r = 1$ is a suitable threshold to remove high redshift galaxies is seen by inspection to figure 3 where we have applied background subtraction counts to sample S2-A up to 400 kpc. The observed lack of excess signal beyond $g - r = 1$ shows that our method is effective in detecting companion galaxies in the colour range $-0.4 < g - r < 1$. This cut is also convenient according to determinations of satellite colours in semianalytic models of galaxy formation (Font et al. 2008) and galaxies in groups in SDSS-DR2 data (Weinmann et al. 2006). Given that we applied a colour cut $g - r < 1$ for galaxies in the photometric sample (section 2.1), the same constraint is requested for galaxies in the mock catalogue. We acknowledge that this cutoff of satellite colours is also present in our background subtraction results as can be appreciated in figure 3, giving confidence that this is a convenient choice. In figure 4 we show the resulting profiles for different ranges in satellite luminosities, where it can be seen that fainter satellites are more concentrated. The maximum projected distance, however, is similar in the three luminosity bins. Due to the K-correction term, distant galaxies in the background have observed red colours, so that using the previous colour cut at $g - r < 1$ a large fraction of contaminating high redshift objects is likely to be excluded. In figure 5 the projected density profile of all galaxies in the color range $g - r = -0.4$ to $g - r = 1.0$ in the sample S2-A-a is compared with the resulting profile for galaxies with $g - r > 1$. As can be appreciated, the signal is strongly diminished and becomes comparable to the Poisson uncertainty. In order to quantify this, we

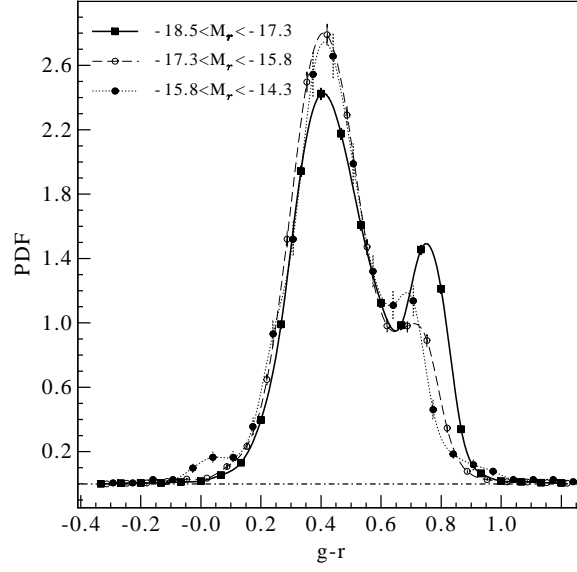


Fig. 2.— Colour distributions of faint galaxies with measured redshifts in SDSS, in three different absolute magnitude intervals. Curves show spline interpolation.

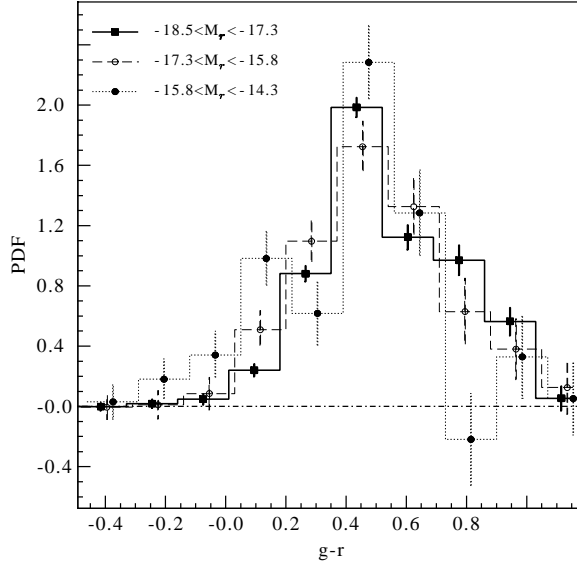


Fig. 3.— Colour distributions of excess counts of companions, in three different magnitude intervals, of bright primaries (sample S2-A) resulting from a background subtraction calculation.

have implemented the adopted colour cut in the mock catalogue by assigning a probability $P(z)$ of a galaxy to be observed with $g - r < 1$ as a function of redshift.

We have used a local background in all cases, in order to account for large scale angular fluctuations in the distribution of faint galaxies. The density profile is observed to be constant beyond 1.5 Mpc (see figure 6) therefore we chose the density in the projected radius interval 2000 – 3000 kpc as the reference level of background galaxy counts. A global background could be used instead, although we argue that a mean number density of galaxies obtained locally is better suited to account for possible irregularities in the number density of background galaxies. We use the redshift of each host to compute the absolute magnitudes corresponding to the excess galaxy counts in different apparent magnitudes, by assuming that these true companion galaxies are at the same redshift than the primary. We compute a composite luminosity distribution by averaging over a sample of primaries with a given set of properties. The number counts per magnitude bin on the resulting composite luminosity distribution estimates are normalized according to the appropriate limits of magnitudes in order to assure completeness, according to:

$$N_i = \sum_j N_{ij} F_j C_j \quad (1)$$

where N_i is the number of galaxies within the i -th magnitude bin for the total ensemble, and N_{ij} is the number of galaxies in that magnitude bin for the j -th primary. The normalization for each magnitude bin is given by the fraction of fields contributing within the completeness limits, C_j , and by the fractional area, F_j , determined by the mask.

3.1. Detailed masks

Since we expect a relatively small number of satellites compared to the total background number counts, several primaries should be used in order to add up the signal over the background noise. Since the number of satellites grows approximately linearly with the number of hosts and Poisson errors scale as the square root of the number of galaxies, a large number of fields is required in order to override the satellite population number over the background counts. In table 1 it can be seen that all samples comprise thousands of primaries, and in particular, the smallest sample (S2-B) contains nearly 5000 host galaxies. Fields of galaxies are extracted from the NYU-VAGC around the primary galaxies. The survey area from which the data is drawn has not, however, a simple geometry, and the detailed structure of holes and borders is an additional problem for the method used in this work. While the external borders are relatively simple, the survey has small disconnected

holes of a variety of shapes. The origin of these holes relies on the presence of several bright objects which blanket the background galaxies, in particular the faint ones. The most important are stars in our galaxy, but we can also mention the trails of solar system objects or artificial satellites, cosmic rays, etc. Moreover, in certain cases, there is a regular pattern of holes, sometimes associated to an incomplete structure of stripes. Therefore, a mask must be built for each of the fields, in order to correctly account for the effective areas used in the method. In figure 7 we show the case of a field containing several holes, some of them near the borders of the area covering 3 Mpc projected radius of the field. The construction of the mask is based on the ansatz that, on a coarse resolution, faint galaxies resemble a dense uniform background so that the holes can be directly associated to the absence of faint objects in a patch of the sky. In order to identify a region without faint galaxies we use a Monte Carlo method which consist in determining faint galaxy distances to uniformly distributed random points within the area considered. We have adopted a percolation radius r_0 equal to a fraction of the mean angular galaxy separation $\langle D \rangle$ in each field. The value of this threshold was obtained by diluting several realizations of complete and dense fields of galaxies, and retrieving in each case the ideal limiting value for the percolation radius. We have checked that this procedure yields reliable results in a large number of cases. An example of the result of such a procedure is shown in figure 7.

4. Results: statistical properties of satellite galaxies

4.1. Determination of projected radial distributions

Although it would be desirable to consider satellites as close as possible to the primary galaxies, there are systematic detection biases that strongly limit this possibility. It is well known that in the SDSS pipeline external parts of large galaxies are often confused as many faint fake galaxies. The deblending process is a difficult task, specially in late-type galaxies where rich luminosity patterns are present on the disk, inducing an artificial neighbor excess close to the primaries. We have also observed that close to primaries, the detection of faint objects can be strongly biased due to several facts such as obscuration, confusion, etc. Galaxies behind bright galaxy discs could also be covered by intrinsic absorption, producing significative changes in the observed magnitudes. To avoid these problems, we have adopted a minimum distance of 100 kpc to primaries for our analysis assuring reliable and systematic-free samples of faint objects.

We considered galaxies in projected radial distance bins from the corresponding primaries to compute the averaged density profile for the different samples. The radial bins are chosen so that all the resulting rings have the same area. This partition allows to explore the

inner region with more detail. In figure 6 we show the density profile of samples S1-A-a and S2-A-a corresponding to all primaries with $-21.5 < M_r < -20.5$ and $-22.0 < M_r < -21.5$ respectively, without restrictions in the colours of primaries nor satellites. It can be appreciated the smoothly declining mean density profiles, although the extent of the overdense region is larger for the brightest hosts. We have also computed the density profiles for red ($0.4 < g - r < 0.8$) and blue ($g - r < 0.4$) companion galaxies of bright primaries with $M_r < -21.5$, (samples S2-A-r and S2-A-b). It can be seen by inspection to figure 6 that the two profiles have a similar spatial extent and radial density profiles.

We have fitted power law functions to the radial density profiles $\rho(r_p) = Ar_p^{-\gamma}$. The resulting values of the profile slope γ are given in table 2 where it can be seen that the companion galaxies of primaries show in general a concentrated distribution.

4.2. Mean number of satellites and luminosity distributions

We detect a significant excess of galaxies up to a maximum projected radius R_{max} varying in the range 300 to 1500 kpc depending on the primary sample. Within R_{max} , we computed the mean number of satellites $\langle N_s \rangle$ in the magnitude range $M_r < -14.5$ for all primary samples, and show the results in table 2. No galaxies were included closer than 100 kpc in projection to the primaries, nor extremely red satellites ($g - r > 1$), since both restrictions were applied in the computations as previously explained. We estimate $\langle N_s \rangle$ for a given sample as:

$$\langle N_s \rangle = \frac{1}{N_p} \sum_{j=1}^n N_{in}^j - \frac{1}{A} N_{out}^j, \quad (2)$$

where N_p is the number of primaries in the sample, N_{in}^j is the number of galaxies inside the inner ring of the j -th field, and N_{out}^j is the number of galaxies inside the chosen outer ring. The area of the background, corrected by the mask, is A times the area enclosed between the chosen radius of the signal inner region. The isolation condition ensures that bright galaxies chosen as centers are somewhat separated from other luminous galaxies, and is intended for selecting a given group of galaxies with similar properties, but does not affect the calculation of the luminosity function, given that it includes satellites at most as bright as $M_s = M_p + 2$. The faintest possible in sample S0 has an absolute magnitude $M_p = -20.5$, so that no satellites with $M_s < -18.5$ are expected to be found in the spectroscopic sample. If galaxies brighter than this limit are considered, the sample of satellites would not be complete, so we limit the study of satellites to the range $-18.5 < r < -14.5$. We assign uncertainty

estimates to the mean number of satellites using Poisson errors resulting from the number counts of galaxies within R_{max} from the primaries and the expected number of background galaxies:

$$\epsilon = \frac{1}{N_p} \sqrt{\sum_{j=1}^n N_{in}^j + \frac{1}{A} N_{out}^j}. \quad (3)$$

We find that the number of satellites depends on primary luminosity. As can be seen in table 2, sample S1 has on typically 1 satellite within the selection windows of color and magnitude used. This number increases to nearly 7 satellites on average for sample S2, except for red ($0.4 < g - r < 1.0$) satellites. This result is consistent with that of Macciò et al. (2010), who study numerical simulations of Milky Way sized haloes as predicted by Cold Dark Matter based models of galaxy formation and find that the number of satellite galaxies increase with halo mass. On the other hand, the number of companion objects of primaries on the same luminosity interval has no a clear dependence with satellite $g - r$ colour index. For the sample of bright and red primaries (S2-R), the number of blue satellites is significantly larger than the number of faint red satellites. For blue primaries, though, the number of blue and red satellites are indistinguishable from each other.

In the computation of the luminosity distribution, a convenient normalization is set for each magnitude bin, so that the mean number of satellites per magnitude interval per primary is obtained. This was achieved by dividing the number counts of excess galaxies by the number of contributing primaries in each magnitude bin. We performed Schechter fits (Schechter 1976) to the differential histograms of magnitude distributions, and computed the faint end slopes, given in table 2.

The results shown in table 2 show a better signal to noise ratio as more primaries comprise the subsamples. Bright primaries ($M_r < -21.5$) host on average 7 satellites while low luminosity primaries ($-21.5 < M_r < -20.5$) host a mean of only 1 satellite galaxy per primary. In figure 8 we show the r -band luminosity distribution of satellites around bright primaries ($M_r < -21.5$) and primaries with intermediate luminosities ($-21.5 < M_r < -20.5$, sample S1). We also show in this Figure Schechter function fits with faint end slope parameters $-0.8 < \alpha < -1.5$, obtained using a maximum likelihood method. These luminosity functions indicate a lack of a dominant population of faint satellites, which would be reflected in much larger negative values of the α parameter. These results contrast with those obtained for groups/clusters of galaxies (Popesso et al. 2005; González et al. 2006), where the faint component contribution $M_r > -18$. to a double Schechter fitting gives slope values as steep as $\alpha \sim -2$.

sample	$\langle N_s \rangle$	α	γ
S0-A-a	1.62 ± 0.78	-1.0 ± 0.3	-2.0 ± 0.2
S0-A-r	1.12 ± 0.35	-1.0 ± 0.3	-2.1 ± 0.5
S0-A-b	1.19 ± 0.33	-1.0 ± 0.3	-1.8 ± 0.4
S1-A-a	1.18 ± 0.28	-1.0 ± 0.3	-2.4 ± 0.3
S1-A-r	1.12 ± 0.33	-1.0 ± 0.3	-2.0 ± 2.0
S1-A-b	0.79 ± 0.44	-1.0 ± 0.3	-1.9 ± 0.5
S2-A-a	7.14 ± 2.66	-1.3 ± 0.3	-1.5 ± 0.4
S2-A-r	2.00 ± 1.89	-1.1 ± 0.3	-1.5 ± 0.7
S2-A-b	6.59 ± 1.41	-1.1 ± 0.3	-1.6 ± 0.3
S2-R-a	18.18 ± 5.39	-1.2 ± 0.2	-1.1 ± 0.6
S2-R-r	4.87 ± 3.09	-1.2 ± 0.2	-0.8 ± 0.7
S2-R-b	10.82 ± 0.71	-1.1 ± 0.2	-1.8 ± 0.2
S2-B-a	5.23 ± 1.83	-1.0 ± 0.3	-1.9 ± 0.5
S2-B-r	3.22 ± 1.00	-1.0 ± 0.3	-2.1 ± 0.7
S2-B-b	2.93 ± 1.65	-1.1 ± 0.3	-1.5 ± 0.6

Table 2: Number of satellites for each sample, and fit parameters for their background subtraction derived projected density profile and luminosity function. The mean number of satellites per host $\langle N_s \rangle$ was calculated in the r -band. Errors are calculated as described in section 3. In all cases, primary redshifts lie in the range $0.03 < z < 0.10$ and the indicated number of satellites include objects in the magnitude range $-18.5 < M < -14.5$.

We have also analyzed the dependence of the results on primary colour index. As mentioned in section 2.1 we have used the threshold $g - r = 0.8$ to divide the samples of primaries. Similarly, we find a larger population of satellites associated to red hosts, with a slightly steeper luminosity distribution at the faint end (figure 9). We have studied the radial density profiles of red and blue satellites around the different samples of primaries, finding that the system of blue satellites is in all cases more extended than that the red ones by approximately 30%. Luminosity distributions of red and blue satellites are shown for the brightest hosts in figure 10. We also computed a colour–magnitude diagram for the satellites obtained by means of applying the background subtraction method simultaneously to these two variables. The results are shown in figure 11 for sample S2-A-a, where it can be appreciated the smooth extension of the spectroscopic data onto fainter objects obtained by our statistical approach.

5. Testing the method with numerical simulations

The success of a background subtraction method relies on the signal-to-background strength from satellites around bright galaxies, providing the overdensity enhancement obtained in the stacking procedure. However, the superposition of large scale structures projected onto the sky could affect the uniformity of the background. In order to estimate the ability of the method to correctly reproduce the actual distributions of satellite galaxies in SDSS-DR7 data, we have tested it on a mock catalogue derived from a numerical simulation using similar conditions than that applied to the observations. We constructed the mock catalogue within a $\pi/2$ steradians light-cone, based on a semianalytic model of galaxy formation (Croton et al. 2006) at redshift zero in the Millennium simulation (Springel et al. 2005), which is publicly available from the German Virtual Observatory ¹. This solid angle corresponds to approximately half the area covered by the spectroscopic DR7 catalogue of galaxies and the $z = 0$ snapshot was replicated 8 times along the axes to achieve a suitable depth.

Since the output of the semianalytic model includes magnitudes in the *ugriz* photometric system, the mock spectroscopic catalogue is obtained directly by selecting galaxies brighter than the limiting apparent magnitude of the Sloan spectroscopic galaxy catalogue, $r=17.77$. From the mock spectroscopic catalogue we extract a sample of mock primaries using similar criteria than in section 2 which will be used as centers in the following analysis. For each galaxy, a redshift is assigned by placing a fiducial observer at one corner, and determining

¹<http://www.g-vo.org>

the comoving distance to the observer and the peculiar velocity of the galaxy. The evolution corrected r -band magnitude is:

$$M_r = -2.5 \log(L) + E - 5 \log(h),$$

where E is given by Blanton et al. (2003).

For the adopted r -band limiting magnitude 21.5 of the photometric sample, the maximum redshift of the mock should be 1.2, corresponding approximately to the distance at which an intrinsically luminous galaxy is observable within the absolute magnitude range explored, $-18.5 < M_r < -14.5$. Although the lack of evolution in both galaxies and structure is a drawback of the mock catalogue, it serves as a strong test of the method given that in this case there is a larger clustering amplitude of high redshift structures (i.e. more structures along the line of sight) compared to a mock catalogue with consistent evolution in clustering.

Since we have adopted a colour cut $g - r < 1$ in SDSS data to reduce background noise, we have performed an appropriate noise reduction in the mock catalogue using a Monte Carlo procedure in order to reproduce the conditions of the observations. We have considered photometric redshifts obtained by O’Mill et al. (2010) (private communication) for the SDSS-DR7 galaxy sample to derive the fraction $P(z)$ of galaxies with observed colour index $g - r < 1$ as a function of redshift. A suitable fit to this probability is given by $P(z) = 1 - 2.381(z - 0.08)$ which rejects about half the galaxies with $g - r > 1$ at $z \sim 0.3$. We have adopted this statistical procedure instead of a direct filtering of galaxies by the observed colour in the photometric mock catalogue, given that this would be model dependent, also requiring reliable K correction for the semianalytic galaxies. We also checked that our results are not strongly dependent on the precise assumed $P(z)$, so that little modifications in the fit have minimum impact in the obtained radial and luminosity distributions.

We have firstly tested if the galaxy density profile around primaries derived by the background subtraction method is able to reproduce the actual projected 3D profile. For this aim we have computed the projected radial distribution of galaxies around centers in the mock catalogue using the real space positions in order to test the reproducibility of the results through the background subtraction method. In figure 12 we show the good agreement of the projected 3D and background subtraction derived profiles, indicating that the method is effective in recovering the true projected profile of companion galaxies. Nevertheless, the profile derived through the background subtraction method exhibits larger fluctuations, due to the larger statistical uncertainty determination. By comparison of figure 12 and figure 6 we can also appreciate a good agreement between the projected galaxy density profiles around primaries in the mock catalogue and the observations (sample S0).

The luminosity distribution of satellite galaxies were computed using the halo membership and galaxy luminosities in the mock catalogue, and compared to the luminosity distribution of galaxies obtained with the background subtraction in the region where the overdensity is observed. The cumulative luminosity distribution obtained through the background subtraction procedure reproduces the true underlying distribution remarkably well, as can be appreciated in figure 13. We also display in the inset of this Figure the differential distributions, which also present a general consistency. The method also succeeds in reproducing the discontinuity at $M_r \approx -17.6$, due to the absolute limiting magnitude in the parent semianalytic galaxy catalogue.

These tests discard the possibility that background structures affect the shape of the obtained luminosity distributions, so that the faint end slopes are computed on firm statistical basis. We stress the fact, however, that this procedure is reliable provided that adequate selection criteria have been imposed to the data. Since primary galaxies in our samples span a redshift range much smaller than most of galaxies contributing to background counts, the procedure used to compute radial and luminosity distributions performs in convenient conditions, as our tests in the mock catalogue have shown. This result is in conformity with previous tests of the method in less favourable conditions as in the determination of cluster luminosity functions (Valotto et al. 2001; Muñoz et al. 2009).

6. Conclusions

We have carried out different statistical analyses to infer properties of faint satellite galaxies associated to bright primaries taken from SDSS with redshift $z < 0.1$. To this end, we have implemented a background subtraction method on faint galaxies with photometric information, that are close in projection to galaxies with measured redshifts. We have used a mock galaxy catalogue based on a semianalytic model of galaxy formation from the Millenium simulation to test the method with similar conditions than in the observational data. According to the results of the tests performed, the method is able to provide a good estimation of the true distributions of luminosities and projected radial galaxy density by distances to the host (figure 12 and figure 13). In our mock catalogue we test how the projection of background structures affect our measurement in a worst case scenario. We conclude that these structures does not affect the shape of the luminosity distribution, provided that central galaxies are sufficiently bright ($M_p < -20.5$) and isolated, and a colour cut $g - r < 1$. is imposed. We also find important to define an adequate maximum radius consistent with the projected extension of the mean excess counts for a given sample of primaries.

In all samples of primaries (defined in table 1) we detect an excess of faint galaxy counts and we can determine statistically the properties of companion objects associated to the central galaxy. We find that the radial density profiles of satellites are consistent with power laws of the form $\rho(r_p) = Ar_p^{-\gamma}$, with $-2.6 \lesssim \gamma \lesssim 1.5$ and that the maximum extent and amplitude of the overdensity depends on the primary luminosity and colour (see figure 6, as well as on galaxy luminosity (figure 4). The dependence of the number of satellites with $M_r < -14.5$ on host luminosity is strong: bright primaries with $M_r < -21.5$ host on average approximately 6 satellites, which is reduced to ~ 1 satellite for $-21.5 < M_r < -20.5$ primary (table 2).

The redshift range of the spectroscopic sample and the apparent magnitude limit of the photometric catalogue allows to obtain luminosity distributions in the range $-18.5 < M_r < -14.5$. The derived luminosity distributions can be well described by Schechter function fits (figure 8). Our findings indicate that faint end slopes of the satellite luminosity functions are nearly flat or slightly rising ($\alpha > -1.3$). This is in agreement with the luminosity distributions of galaxies in the local group, in the same magnitude range (Mateo 1998). This result is valid for all samples and indicates that the population of satellites of bright isolated primaries are consistent with the nearly flat faint end slope of the global luminosity function as derived for the SDSS data (Blanton et al. 2003; Baldry et al. 2005; Montero-Dorta & Prada 2009). These findings contrast with the results obtained by similar methods in samples of clusters and groups where a significantly steep function is obtained ($\alpha \sim -2$ to -1.5 , e.g. de Propris et al. 1995; Popesso et al. 2005; González et al. 2006). These results are expected, given the evidence from semianalytic models of galaxy formation that suggest that the total mass of a dark matter halo determines the normalization and shape of the luminosity function (Macciò et al. 2010).

This work was partially supported by the Consejo Nacional de Investigaciones Científicas y Técnicas (CONICET), and the Secretaría de Ciencia y Tecnología, Universidad Nacional de Córdoba, Argentina. We acknowledge Dr. Carlos Gutierrez and Dr. Nelson Padilla for useful suggestions. We acknowledge Lic. Ana O’Mill for providing data on photometric redshifts. Funding for the SDSS and SDSS-II has been provided by the Alfred P. Sloan Foundation, the Participating Institutions, the National Science Foundation, the U.S. Department of Energy, the National Aeronautics and Space Administration, the Japanese Monbukagakusho, the Max Planck Society, and the Higher Education Funding Council for England. The SDSS Web Site is <http://www.sdss.org/>. The SDSS is managed by the Astrophysical Research Consortium for the Participating Institutions. The of the Royal Astronomical Society Participating Institutions are the American Museum of Natural History, Astrophysical Institute Potsdam, University of Basel, University of Cambridge, Case Western

Reserve University, University of Chicago, Drexel University, Fermilab, the Institute for Advanced Study, the Japan Participation Group, Johns Hopkins University, the Joint Institute for Nuclear Astrophysics, the Kavli Institute for Particle Astrophysics and Cosmology, the Korean Scientist Group, the Chinese Academy of Sciences (LAMOST), Los Alamos National Laboratory, the Max-Planck-Institute for Astronomy (MPIA), the Max-Planck-Institute for Astrophysics (MPA), New Mexico State University, Ohio State University, University of Pittsburgh, University of Portsmouth, Princeton University, the United States Naval Observatory, and the University of Washington. The Millenium Run simulation used in this paper was carried out by the Virgo Supercomputing Consortium at the Computer Centre of the Max-Planck Society in Garching. The semi-analytic galaxy catalogue is publicly available at <http://www.mpa-garching.mpg.de/galform/agnpaper>.

REFERENCES

- Abazajian, K. N., et al. 2009, *ApJS*, 182, 543
- Agustsson, I., & Brainerd, T. G. 2010, *ApJ*, 709, 1321
- Andreon, S., Punzi, G., & Grado, A. 2005, *MNRAS*, 360, 727
- Blanton, M. R., et al. 2003, *ApJ*, 592, 819
- Baldry, I. K., et al. 2005, *MNRAS*, 358, 441
- Barkhouse, W. A., Yee, H. K. C., & Lpez-Cruz, O. 2007, *ApJ*, 671, 1471
- Baugh, C. M. 2006, *Reports of Progress in Physics*, 69, 3101
- Benson, A. J. ????, *Phys. Rep.*
- Benson, A. J., Bower, R. G., Frenk, C. S., Lacey, C. G., Baugh, C. M., & Cole, S. 2003, *ApJ*, 599, 38
- Bertschinger, E. 1994, *Physica D Nonlinear Phenomena*, 77, 354
- Blanton, M. R., Lin, H., Lupton, R. H., Maley, F. M., Young, N., Zehavi, I., & Loveday, J. 2003, *AJ*, 125, 2276
- Blanton, M. R., et al. 2005, *AJ*, 129, 2562
- Chen, J., Kravtsov, A. V., Prada, F., Sheldon, E. S., Klypin, A. A., Blanton, M. R., Brinkmann, J., & Thakar, A. R. 2006, *ApJ*, 647, 86

- Christlein, D. 2000, *ApJ*, 545, 145
- Cole, S., Aragon-Salamanca, A., Frenk, C. S., Navarro, J. F., & Zepf, S. E. 1994, *MNRAS*, 271, 781
- Cooray, A., & Milosavljevic, M. 2005, *ApJ*, 627, L85
- Cooray, A., & Sheth, R. 2002, *Physics Reports*, 372, 1
- Croton, D. J., et al. 2006, *MNRAS*, 365, 11
- de Propriis, R., Pritchet, C. J., Harris, W. E., & McClure, R. D. 1995, *ApJ*, 450, 534
- Font, A. S., et al. 2008, *MNRAS*, 389, 1619
- Fukugita, M., Ichikawa, T., Gunn, J. E., Doi, M., Shimasaku, K., & Schneider, D. P. 1996, *AJ*, 111, 1748
- González, R. E., Lares, M., Lambas, D. G., & Valotto, C. 2006, *A&A*, 445, 51
- Gunn, J. E., Siegmund, W. A., Mannery, E. J., Owen, R. E., Hull, C. L., Leger, R. F., & Carey, L. N. 2006, *AJ*, 131, 2332
- Jones, C., & Forman, W. 1984, *ApJ*, 276, 38
- Kang, X., Jing, Y. P., & Silk, J. 2006, *ApJ*, 648, 820
- Khochfar, S., & Silk, J. 2009, *MNRAS*, 397, 506
- Klypin, A., Kravtsov, A. V., Valenzuela, O., & Prada, F. 1999, *ApJ*, 522, 82
- Koposov, S., et al. 2008, *ApJ*, 686, 279
- Kravtsov, A. V., Gnedin, O. Y., & Klypin, A. A. 2004, *ApJ*, 609, 482
- Lin, Y., Mohr, J. J., & Stanford, S. A. 2004, *ApJ*, 610, 745
- Liu, F. S., Mao, S., Deng, Z. G., Xia, X. Y., & Wen, Z. L. 2009, *MNRAS*, 396, 2003
- Lupton, R., Gunn, J. E., Ivezić, Z., Knapp, G. R., & Kent, S. 2001, in *Astronomical Society of the Pacific Conference Series*, Vol. 238, *Astronomical Data Analysis Software and Systems X*, ed. F. R. Harnden Jr., F. A. Primini, & H. E. Payne, 269–+
- Macciò, A. V., Kang, X., Fontanot, F., Somerville, R. S., Koposov, S., & Monaco, P. 2010, *MNRAS*, 402, 1995

- Mateo, M. L. 1998, *ARA&A*, 36, 435
- Montero-Dorta, A. D., & Prada, F. 2009, *MNRAS*, 399, 1106
- Moore, B., Ghigna, S., Governato, F., Lake, G., Quinn, T., Stadel, J., & Tozzi, P. 1999, *ApJ*, 524, L19
- Muñoz, R. P., Padilla, N. D., & Barrientos, L. F. 2009, *MNRAS*, 392, 655
- Nichol, R. C., Miller, C. J., & Goto, T. 2003, *apss*, 285, 157
- Oemler, A. 1974, *ApJ*, 194, 1
- Okamoto, T., Frenk, C. S., Jenkins, A., & Theuns, T. 2010, *MNRAS*, 406, 208
- O’Mill, A., Duplancic, F., Lambas, D. G., & Sodré, L. 2010, *MNRAS*, submitted to, 00
- Ostriker, J. P., & Tremaine, S. D. 1975, *ApJ*, 202, L113
- Pimbblet, K. A. 2008, Are dumbbell brightest cluster members signposts to galaxy cluster activity?, <http://adsabs.harvard.edu/abs/2008arXiv0808.2093P>
- Popesso, P., Böhringer, H., & Voges, W. 2005, in *Multiwavelength Mapping of Galaxy Formation and Evolution*, ed. A. Renzini & R. Bender, 444–+
- Sales, L., & Lambas, D. G. 2005, *MNRAS*, 356, 1045
- Schechter, P. 1976, *ApJ*, 203, 297
- Simon, J. D., & Geha, M. 2007, *ApJ*, 670, 313
- Skibba, R. A., van den Bosch, F. C., Yang, X., More, S., Mo, H., & Fontanot, F. 2010, *MNRAS*, 1465
- Smith, G. P., Kneib, J., Smail, I., Mazzotta, P., Ebeling, H., & Czoske, O. 2005, *MNRAS*, 359, 417
- Smith, J. A., et al. 2002, *AJ*, 123, 2121
- Springel, V., et al. 2005, *Nature*, 435, 629
- Stoughton, C., Lupton, R. H., Bernardi, M., Blanton, M. R., Burles, S., Castander, F. J., Connolly, A. J., & Eisenstein, D. J. 2002, *AJ*, 123, 485
- Strauss, M. A., Weinberg, D. H., Lupton, R. H., Narayanan, V. K., Annis, J., Bernardi, M., Blanton, M., & Burles, S. 2002, *AJ*, 124, 1810

- Strigari, L. E., Bullock, J. S., Kaplinghat, M., Diemand, J., Kuhlen, M., & Madau, P. 2007, *ApJ*, 669, 676
- Tollerud, E. J., Bullock, J. S., Strigari, L. E., & Willman, B. 2008, 688, 277
- Trentham, N., & Tully, R. B. 2002, *MNRAS*, 335, 712
- . 2009, *MNRAS*, 398, 722
- Tully, R. B., & Trentham, N. 2008, *AJ*, 135, 1488
- Vale, A., & Ostriker, J. P. 2006, *MNRAS*, 371, 1173
- Valotto, C. A., Moore, B., & Lambas, D. G. 2001, *ApJ*, 546, 157
- Viola, M., Monaco, P., Borgani, S., Murante, G., & Tornatore, L. 2008, *MNRAS*, 383, 777
- Weinmann, S. M., van den Bosch, F. C., Yang, X., & Mo, H. J. 2006, *MNRAS*, 366, 2
- White, S. D. M. 1976, *MNRAS*, 174, 19
- White, S. D. M., & Frenk, C. S. 1991, *ApJ*, 379, 52
- Willman, B., Dalcanton, J., Ivezić, Z., Jackson, T., Lupton, R., Brinkmann, J., Hennessey, G., & Hindsley, R. 2002, *ApJ*, 123, 848

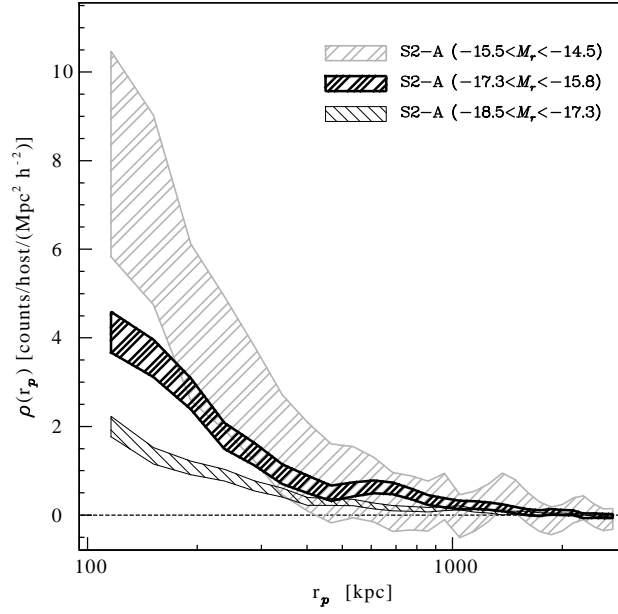


Fig. 4.— Density profile of S2-A sample selected by satellite luminosity. Fainter satellites show a steeper density profile, which extends up to approximately 400 kpc. Brighter satellites show a greater spatial extension, but smaller excess.

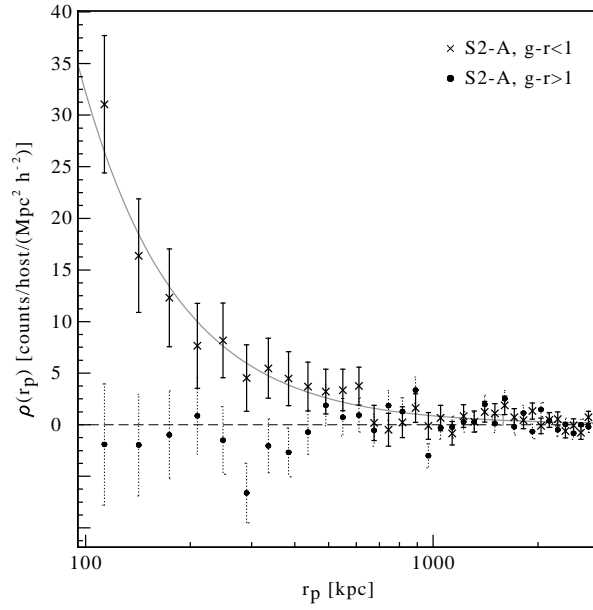


Fig. 5.— Mean projected density profile of galaxies with $g - r < 1.0$ around primaries with $M_r < -21.5$ (sample S2). For comparison, the long dashed lines show $1-\sigma$ uncertainties obtained for galaxies with $g - r > 1.0$ (mainly background objects) around the same primaries.

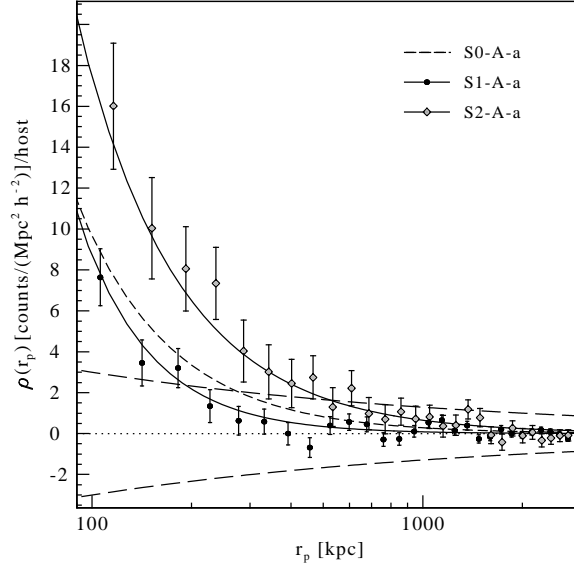


Fig. 6.— Density profile of excess galaxies around primaries in samples S0-A-a, S1-A-a, and S2-A-a. For simplicity, only the power law fit is shown for sample S0-A-a, along with the uncertainty amplitude in long dashed lines.

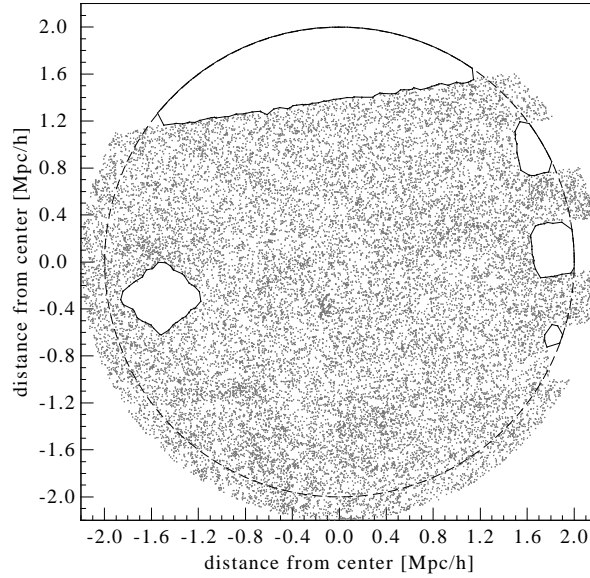


Fig. 7.— Example of a field with a complex structure of holes and borders, and the corresponding mask constructed using the Monte Carlo procedure, as described in section 3.1.

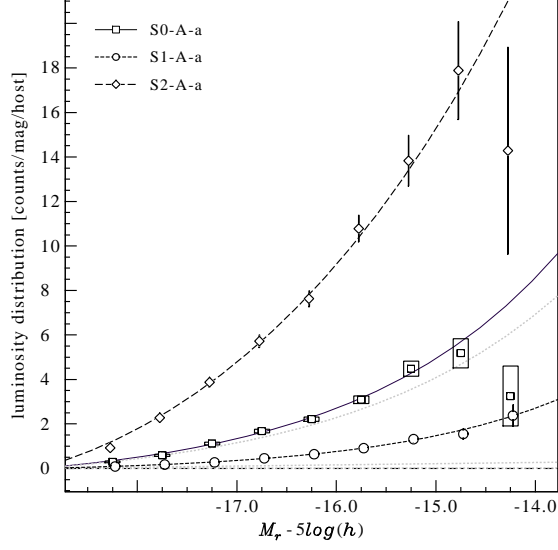


Fig. 8.— Cumulative luminosity distributions of excess galaxies around primaries in the three defined samples (dubbed S0, S1 and S2). Lines represent the best Schechter function fits to the obtained distributions. Dotted lines show, for comparison, Schechter functions with the same ϕ_0 and M_* parameters than sample *S0 – A – a*, but with faint end slopes values -1.5 , -1.0 and -0.5 .

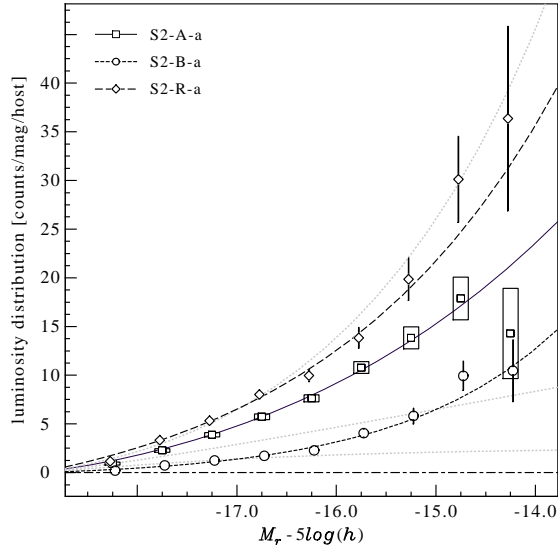


Fig. 9.— Cumulative luminosity distributions of excess galaxies around bright primaries ($M_r < -21.5$). Luminosity distributions for red and blue hosts (with a colour cut in $g - r = 0.8$) are also shown. Dotted lines show the Schechter functions with α parameters equal to -1.5 , -1.0 and -0.5 .

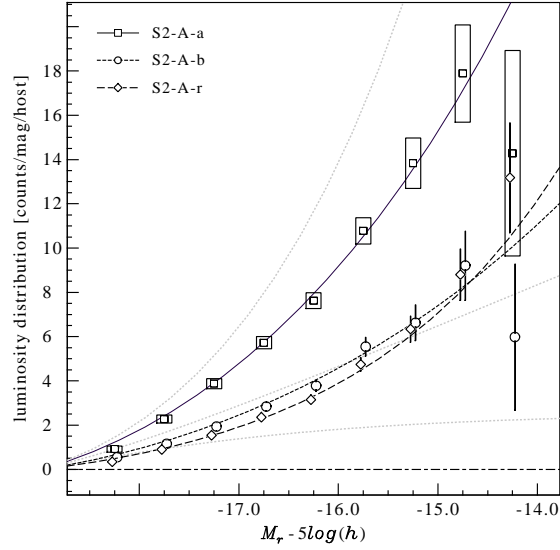


Fig. 10.— Cumulative luminosity distributions of blue ($0.0 < g - r < 0.4$), red ($0.4 < g - r < 0.8$) and all ($0.0 < g - r < 0.8$) excess galaxies around bright primaries in sample S2-A. Dotted lines are cumulative Schechter functions with different faint end slopes (-1.5 , -1.0 and -0.5) that share the same M_* and ϕ_* parameters than sample S2-A-a (solid line).

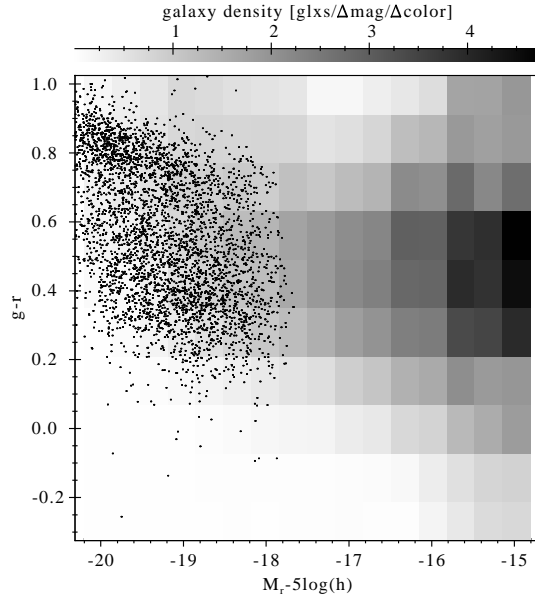


Fig. 11.— Colour-magnitude distribution of excess counts of $-18 < M_r < -15$ companions of bright primaries (sample S2-A) resulting from a background subtraction calculation.

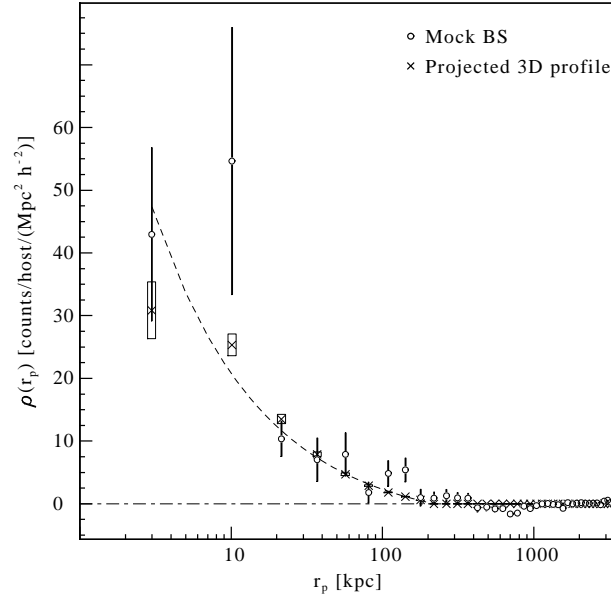


Fig. 12.— Projected density profile of galaxies around primaries in the mock catalogue. Open circles correspond to results obtained by the background subtraction method, and filled circles correspond to the projection of the 3D density profile within the halos of each primary.

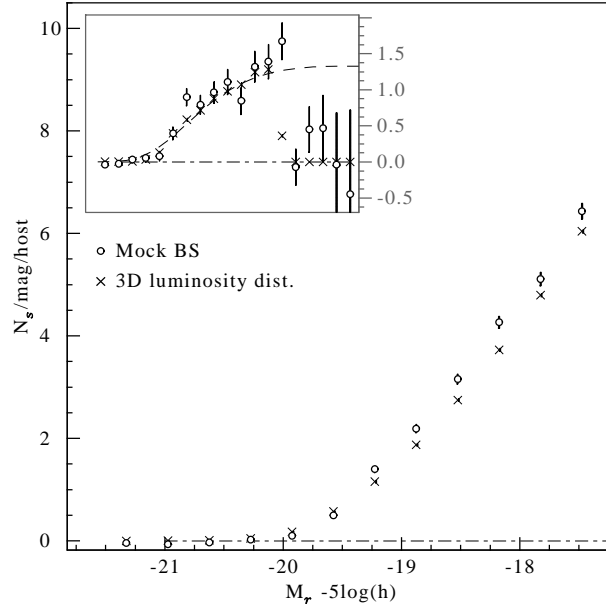


Fig. 13.— Luminosity distribution of galaxies around primaries in the mock catalogue. Open circles correspond to the results from the background subtraction method. Filled circles are the actual luminosity distribution of satellites within the halos of primary.